Transport of Space Environment Electrons: A Simplified Rapid-Analysis Computational Procedure

John E. Nealy
Old Dominion University, Norfolk, Virginia

Brooke M. Anderson
Swales Aerospace Corporation, Hampton, Virginia

Francis Cucinotta
Lyndon B. Johnson Space Center, Houston, Texas, francis.cucinotta@unlv.edu

John W. Wilson
Langley Research Center, Hampton, Virginia

Robert Katz
University of Nebraska-Lincoln, rkatz2@unl.edu

See next page for additional authors

Authors

John E. Nealy, Brooke M. Anderson, Francis Cucinotta, John W. Wilson, Robert Katz, and C. K. Chang

NASA/TP-2002-211448

Transport of Space Environment Electrons: A Simplified Rapid-Analysis Computational Procedure

John E. Nealy
Old Dominion University, Norfolk, Virginia

Brooke M. Anderson
Swales Aerospace Corporation, Hampton, Virginia

Francis A. Cucinotta
Lyndon B. Johnson Space Center, Houston, Texas

John W. Wilson
Langley Research Center, Hampton, Virginia

Robert Katz
University of Nebraska, Lincoln, Nebraska

C. K. Chang
Christopher Newport University, Newport News, Virginia

March 2002

The NASA STI Program Office . . . in Profile

Since its founding, NASA has been dedicated to the advancement of aeronautics and space science. The NASA Scientific and Technical Information (STI) Program Office plays a key part in helping NASA maintain this important role.

The NASA STI Program Office is operated by Langley Research Center, the lead center for NASA's scientific and technical information. The NASA STI Program Office provides access to the NASA STI Database, the largest collection of aeronautical and space science STI in the world. The Program Office is also NASA's institutional mechanism for disseminating the results of its research and development activities. These results are published by NASA in the NASA STI Report Series, which includes the following report types:

- TECHNICAL PUBLICATION. Reports of completed research or a major significant phase of research that present the results of NASA programs and include extensive data or theoretical analysis. Includes compilations of significant scientific and technical data and information deemed to be of continuing reference value. NASA counterpart of peer-reviewed formal professional papers, but having less stringent limitations on manuscript length and extent of graphic presentations.

- TECHNICAL MEMORANDUM. Scientific and technical findings that are preliminary or of specialized interest, e.g., quick release reports, working papers, and bibliographies that contain minimal annotation. Does not contain extensive analysis.

- CONTRACTOR REPORT. Scientific and technical findings by NASA-sponsored contractors and grantees.

- CONFERENCE PUBLICATION. Collected papers from scientific and technical conferences, symposia, seminars, or other meetings sponsored or co-sponsored by NASA.

- SPECIAL PUBLICATION. Scientific, technical, or historical information from NASA programs, projects, and missions, often concerned with subjects having substantial public interest.

- TECHNICAL TRANSLATION. English-language translations of foreign scientific and technical material pertinent to NASA's mission.

Specialized services that complement the STI Program Office's diverse offerings include creating custom thesauri, building customized databases, organizing and publishing research results . . . even providing videos.

For more information about the NASA STI Program Office, see the following:

- Access the NASA STI Program Home Page at *http://www.sti.nasa.gov*

- Email your question via the Internet to help@sti.nasa.gov

- Fax your question to the NASA STI Help Desk at (301) 621-0134

- Telephone the NASA STI Help Desk at (301) 621-0390

- Write to:
  NASA STI Help Desk
  NASA Center for AeroSpace Information
  7121 Standard Drive
  Hanover, MD 21076-1320

NASA/TP-2002-211448

Transport of Space Environment Electrons: A Simplified Rapid-Analysis Computational Procedure

John E. Nealy
Old Dominion University, Norfolk, Virginia

Brooke M. Anderson
Swales Aerospace Corporation, Hampton, Virginia

Francis A. Cucinotta
Lyndon B. Johnson Space Center, Houston, Texas

John W. Wilson
Langley Research Center, Hampton, Virginia

Robert Katz
University of Nebraska, Lincoln, Nebraska

C. K. Chang
Christopher Newport University, Newport News, Virginia

March 2002

Abstract

A computational procedure for describing transport of electrons in condensed media has been formulated for application to effects and exposures from spectral distributions typical of electrons trapped in planetary magnetic fields. The procedure is based on earlier parameterizations established from numerous electron beam experiments. New parameterizations have been derived that logically extend the domain of application to low molecular weight (high hydrogen content) materials and higher energies (~50 MeV). The production and transport of high energy photons (bremsstrahlung) generated in the electron transport processes have also been modeled using tabulated values of photon production cross sections. A primary purpose for developing the procedure has been to provide a means for rapidly performing numerous repetitive calculations essential for electron radiation exposure assessments for complex space structures. Several favorable comparisons have been made with previous calculations for typical space environment spectra, which have indicated that accuracy has not been substantially compromised at the expense of computational speed.

Introduction

The constituents of ionizing radiation fields in the space environment of most importance for effects on human or other biological systems and radiosensitive electronic components are the high-energy nuclei of the galactic cosmic rays (GCR), the energetic light ions of sporadic solar particle events (SPE), and the protons and electrons trapped within magnetic fields associated with a stellar or planetary object. Interactions of these radiations with condensed matter can produce secondary fields of high-energy neutrons and photons. Prediction of the nature of effects caused by such radiations depends upon understanding the manner in which the radiation fields propagate through various materials comprising the media of interest. A comprehensive exposition of various aspects of light and heavy ion transport is given by Wilson et al. (ref. 1) that emphasizes the adequacy of a one-dimensional approximation in the attenuation of such ions in condensed matter. The error is proportional to the second power of beam divergence to radius of curvature of the shield. Mainly, low-energy neutron transport requires added consideration. The much lighter electrons, however, are much more subject to undergo change in their direction of motion when they interact with the charged particles comprising the atoms and molecules of a substance.

An excellent treatment of the various complexities of detailed electron transport is given by Jenkins, Nelson, and Rindi (ref. 2), which is devoted to the analytical description of electron transport by Monte Carlo techniques. Such statistical approaches have the advantage that the physical processes involved may be modeled in detail, and comparisons with controlled experiments are usually very favorable so that when the physical models have been verified, Monte Carlo results are often used as "benchmark" calculations. Some disadvantages of the Monte Carlo approaches are that they often tend to require substantial computer storage and execution time. This is most important in an engineering design environment where optimization processes depend on high-performance computational methods.

The present work describes a formulation in which the philosophy of one-dimensional transport is retained, but modified to try to account for average effects of multiple scattering events and high frequency energy fluctuations. Complex mathematical descriptions of individual collision processes have been replaced with a continuous, deterministic representation. Thus, the computational complexity and

mass storage requirements of Monte Carlo techniques are greatly reduced. Nevertheless, as with most engineering approximation approaches, some aspects of the physical phenomena are not represented, and the range of validity of the approximations invoked should be carefully defined. The purposes of the present study are (1) to describe the formulation of the computational procedure in some detail, along with input data base structure; (2) to compare some results with suitable benchmark calculations and define some limitations and ranges of validity; and (3) to demonstrate by means of sample calculations some representative applications of the procedure.

Electron Transport

Computational Formulation

The paths of sufficiently energetic electrons traveling in condensed media may be roughly approximated by straight-line motion. In the absence of catastrophic interactions (e.g., positron annihilation, nuclear reaction processes), the straight-ahead approximation becomes more favorable with increasing energy. The electron transit through a substance may be characterized by the stopping power $-(dE/dx)$, or loss of energy E, per unit distance x. Approximate stopping power formulas have been developed from first principles, and later extensively refined to incorporate corrections to earlier expressions. An excellent overview on stopping power theory and application in the section by Berger appears in reference 2.

If an electron having initial energy E is assumed to lose its energy continuously in transit, its maximum travel distance or path length R may be found as

$$R(E) = \int_E^0 \left[\frac{1}{\left(\frac{-dE'}{dx} \right)} \right] dE' \tag{1}$$

and is referred to as the Continuous-Slowing-Down-Approximation (CSDA) range, or pathlength. In practice, straggling, and especially multiple scattering, makes the pathlength a complicated set of randomly directed line segments. The actual penetration depth or range of electrons is observed to be less than the CSDA range, with the deficit dependent on both material composition and energy. Tabata, Ito, and Okabe (ref. 3) have developed a parameterization for the practical range of electrons based on experimental tests involving several materials and a broad energy range (0.3 keV to 30 MeV). Tabata explicitly parameterizes the practical (extrapolated) range R_{ex} of an electron in material of atomic number Z and atomic weight A as

$$R_{ex} = a_1 \left[\left(\frac{1}{a_2} \right) \ln \left(1 + a_2 \tau \right) - \left(\frac{a_3 \tau}{1 + a_4 \tau^{a_5}} \right) \right] \tag{2}$$

where $\tau = E/(m_e c^2)$ with m_e as electron rest mass and c the speed of light. The coefficients a_i are given in terms of A, Z, and constants $b_{j=1-9}$ as

a_1	a_2	a_3	a_4	a_5
$b_1 A/Z^{b_2}$	$b_3 Z$	$b_4 - b_5 Z$	$b_6 - b_7 Z$	b_8/Z^{b_9}

With the b_j specified as

b_1	b_2	b_3	b_4	b_5	b_6	b_7	b_8	b_9
0.2335	1.209	0.000178	0.9891	0.000301	1.468	0.0118	1.232	0.109

the formulas may be used to calculate R_{ex} in units of g/cm^2.

The parameterization of reference 3 has been examined as to the relationship with the CSDA range computed from the stopping power tabulations of Berger and Seltzer (ref. 4). Plots of the CSDA stopping powers and corresponding range values are given in figures 1 and 2, respectively, for selected elemental species and for electron energies between 0.01 and 100 MeV. When the parameterized practical ranges are ratioed to the CSDA ranges, values generally less than unity occur over the quoted energy range of applicability for the middle and higher atomic number elements ($Z > \approx 10$), as expected. However, the formulas of reference 3 lead to ratios exceeding unity for these heavier elements at higher energies ($> \approx 20$ MeV). For lower Z elements, the CSDA range is exceeded at even lower energies. Since the formulations of reference 3 are based primarily on data citations for the heavier elements, it was felt that a reevaluation be considered using the observed range ratios for the heavier elements along with a rational extrapolation to higher energies and lower atomic weights.

It is convenient to define the ratio $F_R = R_{ex}/R_{CSDA}$. Plots of the semiempirical functions of reference 3 used in CSDA range ratios suggest that lower order polynomials are suitable functional forms for elements with $Z > \approx 13$. We have parameterized F_R as cubic equations of the form

$$F_R = a(Z)X^3 + b(Z)X^2 + c(Z)X + d(Z) \approx \frac{R_{ex}}{R_{CSDA}} \tag{3}$$

in terms of a normalized energy variable,

$$X \equiv \frac{\left[\log_{10}\left(E_{MeV}\right) - \log_{10}(0.01)\right]}{\left[\log_{10}(100) - \log_{10}(0.01)\right]} \tag{4}$$

It is found that the coefficients exhibit approximately regular variations with Z and may also be represented by simple mathematical functions. Reasonable fits to the coefficients (including rational extension to low atomic numbers) have been found as:

$$a = 0.02258\left(y_Z\right)^2 - 0.13854\left(y_Z\right) + 0.3695 \tag{5}$$

$$b = -0.00605\left(x_Z\right)^3 + 0.04388\left(x_Z\right)^2 + 0.07536\left(x_Z\right) + 0.075 \tag{6}$$

$$c = -0.56\left\{1.0 - \exp\left[-0.0030706\left(y_Z\right)^{4.1514}\right]\right\} \tag{7}$$

$$d = 0.971 - 0.071\left(y_Z\right) \tag{8}$$

with $y_Z = Z^{1/2}$ and $x_Z = y_Z - 1$.

3

In order that the new parameterizations F_R are constrained to be less than or very nearly equal to 1, they are modified by an exponential "filter" such that when F_R approaches 1 at higher energies, the polynomial is suppressed exponentially and replaced with a corresponding approach to unity. The exponential function is of the form

$$\varphi(X) = \exp\left[-A(X)^n\right] \tag{9}$$

where X is the normalized energy variable previously defined. For the present application, the constants A and n are chosen so that the slope of the function is $-80°$ at $\varphi(X) = 0.5$. These constants may then be expressed in terms of a "transition energy variable" X_T as

$$\left. \begin{aligned} n &= 16.364\,X_T \\ A &= 0.69315(X_T)^{-n} \end{aligned} \right\} \tag{10}$$

The transition energies for which these conditions occur are somewhat arbitrary, and have here been selected as a function of atomic number so as to produce a reasonable approach to the CSDA range with increasing energy. The functional form chosen is

$$X_T(Z) = -0.0043438\,X_Z^2 + 0.078366\,X_Z + 0.5753 \tag{11}$$

where $X_Z = Z^{1/2} - 1$. Thus, the final form of the expression for practical (extrapolated) range as used in the present study is

$$R_{\text{ex}}/R_{\text{CSDA}} = F_R(X, Z)\,\varphi(X, Z) + \left[1 - \varphi(X, Z)\right] \tag{12}$$

Graphical representations of the range ratios for the earlier and present formulations are given in figure 3. In this way, the extrapolated range approaches the electron pathlength at high energies, and, for light elemental targets, reaches the asymptote at lower energies.

In order to account for the differences between observed energy dissipation by electrons and that predicted by CSDA, Kobetich and Katz (refs. 5 and 6) have devised a relationship of the form

$$G(E, t) = \frac{d(\eta W)}{dt} \tag{13}$$

where G is the energy dissipation of an electron of initial energy E having residual energy W, after traveling distance t; η is the probability of transmission at distance t. Their parameterization of η in terms of range R is given as

$$\eta = \exp\left[-\left(\frac{qt}{R}\right)^p\right] \tag{14}$$

where

$$\left. \begin{aligned} q &= 0.0059\,Z^{0.98} + 1.1 \\ p &= 1.8(\log_{10} Z)^{-1} + 0.31 \end{aligned} \right\} \tag{15}$$

and is limited to values of $Z > 1$.

4

In the present formulation, the formula for *p* of Kobetich and Katz has been modified as

$$p = 1.2 + 1.3415 \, \exp\left(-0.04723Z\right) \tag{16}$$

to extend the parameterization logically into the neighborhood of $Z = 1$ (where the original formula tends to become indeterminate) and to retain the character of the formula at higher *Z* values. It was found that this modification appeared to be a viable representation. The effects of path-length straggling near the distance at which the electron has lost most of its energy are also parameterized in reference 5 to constrain the dissipation function *G* as

$$G(E, t \geq 0.9R) \;=\; G(E, t = 0.9R)\left[\frac{\eta(t)}{\eta(0.9R)}\right]^{4/p} \tag{17}$$

This expression has been retained in the present formulation.

For a fluence (or flux) of electrons differential in energy, $\phi(E, t{=}0)$—having initial energies *E*, the dose *D*, at depth *t*—is given in terms of the dissipation function (ref. 7) as

$$D(t) = (1/2\pi) \int G(E, t) \, \phi(E, t) \, dE \tag{18}$$

The dose may also be written in terms of the residual energies *W* as

$$D(t) = \int S(W) \, \phi(W, t) \, dW \tag{19}$$

(Note that the energy dissipation function has been derived on the basis of electrons incident on a semi-infinite slab for total solid angle of 2π sr.) Equating the two integrands and dividing each side by differential thickness element *dt* leads to an expression for the electron spectrum at location *t* in terms of the initial spectrum:

$$\phi(W, t) \;=\; (1/2\pi) \, \phi(E, 0) \, G(E, t) \, \frac{S(E)}{\left[S(W)\right]^2} \tag{20}$$

where *S* represents the CSDA stopping power. The residual energy *W* at distance *t*, for an electron of initial energy *E* and having range *R*, is found by solving the equation

$$R_{\text{ex}}(W) = R_{\text{ex}}(E) - t \tag{21}$$

for *W* when the practical range satisfies the condition $R_{\text{ex}}(W) > 0$. This operation is performed numerically in the present algorithm.

As electrons undergo deceleration in transit through condensed matter, energetic photons (bremsstrahlung) are produced that also propagate through the medium and contribute to the general energy deposition (dose). The photons are generally distributed spectrally from very low energies up to the electron energy producing them, and their spectra are related to production cross sections that are dependent on both the atomic composition of the material and the electron energy. When electrons of energy *W* at distance *t* produce photons of energy in the interval between E_ν and $E_\nu + dE_\nu$, the source term ζ (in,

5

for example, units of photons/cm^3-MeV), at distance t in the material, may be written in terms of the differential photon production cross section, $\sigma(W, E_\nu)$

$$\zeta(E_\nu, W) = \int_{E_\nu}^{W(t)} \phi(W', t)\, \sigma(W', E_\nu)\, dW' \tag{22}$$

where $W' \geq E_\nu$. The cross sections $\sigma(W, E_\nu)$ are generally complicated functions of W and E_ν, and material composition. They have been extensively tabulated by Seltzer and Berger (ref. 8) for wide energy ranges and most elements of the periodic chart. The effective production cross sections for a given material are determined in the present calculations by appropriate spline interpolations of the Berger-Seltzer tabulations. Plots of scaled cross sections for selected atomic species are given in figure 4 ((a)–(f)). The differential cross sections have been scaled with multiplication by the factor $E_\nu(\beta/Z)^2$, with β being the ratio of electron speed to the speed of light. Individual curves represent cross section variation for a constant ratio of emitted photon energy to incident electron kinetic energy.

The attenuation of the emitted photons in the material can be characterized by a total extinction coefficient μ_T and the photon differential energy spectrum ϕ_ν at distance t in the medium may be found by using the radiative transfer equation:

$$\phi_\nu(E_\nu, t) = \int \zeta(x, E_\nu)\, \exp\left[-\mu_T(t - x)\right] dx \qquad (t > x) \tag{23}$$

Photon energy deposition contributing to the general ionizing radiation dose may be characterized by an "energy deposition" absorption coefficient μ_E in the calculation of dose due to bremsstrahlung,

$$D_\nu(t) = \int \mu_E E_\nu\, \phi_\nu(E_\nu, t)\, dE_\nu \tag{24}$$

The energy absorption coefficient is generally less than that for total attenuation μ_T. Photon absorption coefficient data used in the present procedure are shown for selected species in figures 5 and 6, and have been taken from the data tabulations of Storm and Israel (ref. 9). The present code formulation assumes all photons generated propagate in the direction of electron motion. This approximation should result in overestimates, or conservative values, for photon energy deposition in a given direction.

Comparisons With Other Calculations

The present computational procedure was used to replicate several calculations performed with other electron transport codes. In what was considered to represent a benchmark comparison, the Monte Carlo code TIGER-P (ref. 10) was used to generate dose versus depth curves in water for electrons and associated bremsstrahlung. An initial spectrum based on the 10-day mission fluence of STS-63 was propagated into the H_2O medium at normal incidence. The results of this generally favorable comparison, along with the initial spectrum, are shown in figure 7.

Another comparison was made for a low Earth orbit (LEO) situation for a representative International Space Station (ISS) environment. The electron spectrum and associated calculation were supplied by W. Atwell, Technical Research Fellow, Boeing Corporation, Houston, Texas (private communication, March 2001), for transport through a semi-infinite aluminum slab (Al slab) geometry for omnidirectional flux subtending 2π sr. A Boeing in-house code developed from a series of Monte Carlo calculations was used to provide the resultant doses with energy deposition evaluated for an H_2O medium. Again, the comparison is very favorable, as is seen in figure 8.

6

A third comparison calculation was made for geostationary Earth orbit (GEO) conditions based on published results of Stassinopoulos (ref. 11) in which the daily omnidirectional integral flux spectrum is tabulated along with resultant doses evaluated for energy deposition in an aluminum medium. Figure 9 shows the results of this comparison. While the electron dose functions compare very favorably, the bremsstrahlung curves exhibit considerable differences. Apparently, the larger photon flux at low thicknesses is a consequence of the differential flux evaluation at low energies. Since the energetic photons are much more penetrating than electrons, an overestimate of the initial low-energy differential electron flux will result in larger bremsstrahlung contributions at greater thicknesses. An investigation of the sensitivity of results on different evaluations of the derivative was not pursued in this study.

Sample Calculations and Results

A description of the program setup, along with examples of optional output, is given here only as an illustration of the existing run process and does not pertain to any specific application. The program requires an input file specifying an initial energy grid and corresponding electron fluxes, differential in energy. A maximum energy (normally the highest energy prescribed for the input spectrum) is also specified. For the present example, the fluence spectrum of the STS-63 mission used previously has been chosen, consisting of 29 spectral points with maximum energy of 6 MeV. (Note that the energy range of validity for the code in general is 0.01 to 100 MeV.) In the course of the electron transport computational procedure, the energy grid points for the electrons are redistributed in accordance with energy loss, with density of grid points being greatest at lower energies to better define the slowing down and stopping processes. The original number of grid points remains constant. The photon energy grid is automatically established for the same number of grid points and increase by logarithmic increments from 0.01 MeV to the initial maximum electron energy, and remains invariant throughout the calculation. As an option, a photon spectrum may also be included as an initial condition; in the present example, initial photon flux is zero.

A second input file defining the material layers (compositions and thicknesses) is also required. The total thickness of the layer and the number of spatial grid points to be included within the layer must be specified. The spatial grid points (normally 15 to 20 values) are automatically distributed logarithmically for more accurate treatment of the photon transport processes in the material. Values representing thicknesses are actually expressed in terms of areal density, g/cm^2 (i.e., density × linear thickness). The material composition must be specified in terms of a distinct number of atomic species (presently 1 to 6) with their respective atomic numbers, atomic weights, and number of atoms of each type in the composite molecular formula. These data are then used in the algorithm to compute molecular weights and atomic densities per unit mass of material. Data for each layer appear sequentially in the material data file; there is presently no limitation on the number of different material layers to be included in a particular calculation. A third and final requisite input file contains all of the atomic data for electron stopping powers, photon production, and attenuation cross sections, and is only changed for updates to basic atomic properties data.

For the present sample calculation the material slab is composed of three layers: a lightweight (Lt), lower molecular weight layer; a heavier (Hv), high molecular weight layer; and a final water layer. A polyurethane, $(C_5H_5NO_2)_n$, has been chosen as the light material, and a hypothetical tungsten-fiberglass composite of assumed composition $(WSiO_2)_n$ represents the heavy layer. (The assumed formula for the composite is based on approximate mass fractions of 0.75 for W and 0.25 for SiO_2.) The water layer is taken as representative of human tissue. Each layer is specified as having areal density of 0.5 g/cm^2.

The electron stopping powers, associated ranges, and photon production and attenuation coefficients are calculated for each material by weighted averaging of the atomic coefficients with respect to the corresponding atomic densities. Figure 10 shows the computed stopping powers and ranges for the three selected materials. The photon total attenuation and energy absorption coefficients are given in figure 11, and the photon production cross sections are shown in figure 12.

Two transport calculations were made for the three-layer combination in which the sequence of light and heavy materials in front of the tissue layer were interchanged. The calculated electron spectra at the material interfaces are shown for the two cases in figure 13. The difference in flux values at the first interface is most notable, whereas the flux incident on the final water layer is very similar. The figure also illustrates the varying electron energy grid as indicated by the location of symbols along the curves. Photon source terms are plotted in figure 14, where photon production at each interface is shown. As expected, photon production decreases as electron energies are degraded or as electrons are stopped. Most notable is the substantially greater photon production in the heavy layer. Corresponding photon fluence spectra at the two interior interfaces are given in figure 15. Largest differences are observed at the lower energies (10 to 100 keV); when the layer sequence is such that the middle ply is the lighter polyurethane, attenuation at higher photon energies is scarcely noticeable for the thickness specified.

The variation of dose (energy deposition) in the three-layer slab combinations is presented in figure 16. It was specified that 20 grid points be used for the first two strata, while only 5 were used for the simulated tissue layer. Again, plot symbols indicate the automatic decadal spacing of the points. The very prominent bremsstrahlung dose in the heavy layer is most evident. When the heavy layer is subjected to the unattenuated environment electrons, relatively more electrons are produced and result in a higher dose in the final tissue layer. For this calculation, the corresponding electron dose variations in the final layer are quite similar for the two cases. However, other calculations for material layers having greater differences in molecular weights have shown larger disparities in final electron tissue dose.

Concluding Remarks

The major advantages of the electron procedure here described are its computational speed along with its versatility with respect to description of transport in arbitrary materials and/or combinations of materials. The capability of generating optional electron and photon energy spectra at preselected spatial locations is another positive feature that would facilitate numerical diagnostic analysis, and allow for special applications where spectral definition is of importance. In its present form, the nominal energy range of validity is 0.01 to 100 MeV, but the user should recognize that the experimental data on which the original formulation was based dealt predominantly with measurements for energies <30 MeV and for materials composed of constituents of intermediate to heavy atomic masses. The rationale for extension to lower atomic weights and somewhat higher energies has been discussed; experimental verification in these domains would be especially helpful, particularly for ultralightweight polymers designed for space flight applications.

The current version of the code is considered well-suited for calculations of electron energy deposition for LEO trapped electrons. For applications involving high-energy beams or the more intense Jovian trapped environment, it would be desirable to incorporate pair production and certain photonuclear processes in the procedure. Such enhancements would necessarily require extension of the existing database, and appropriate modification of the computational grid structure. These improvements are presently being formulated for inclusion in future versions of the procedure.

References

1. Wilson, J. W.; Townsend, L. W.; Schimmerling, W.; Khandelwal, G. S.; Khan, F.; Nealy, J. E.; Cucinotta, F. A.; Simonsen, L. C.; Shinn, J. L.; and Norbury, J. W.: *Transport Methods and Interactions for Space Radiations.* NASA RP-1257, 1991.

2. Jenkins, T. M.; Nelson, W. R.; and Rindi, A., eds.: *Monte Carlo Transport for Electrons and Photons.* Plenum Press, 1989.

3. Tabata, T.; Ito, R.; and Okabe, S.: Generalized Semiempirical Equations for the Extrapolated Range of Electrons. *Nucl. Inst. & Meth.*, vol. 103, 1972, pp. 85–91.

4. Berger, M. J.; and Seltzer, S. M.: *Stopping Powers and Ranges of Electrons and Positrons.* Rep. NBSIR 82-2550, U.S. Dept. of Commerce, Aug. 1982.

5. Kobetich, E. J.; and Katz, Robert: Energy Deposition by Electron Beams and δ Rays. *Phys. Rev.*, vol. 170, no. 2, June 1968, pp. 391–396.

6. Kobetich, E. J.; and Katz, R.: Electron Energy Dissipation. *Nucl. Inst. & Meth.*, vol. 71, 1969, pp. 226–230.

7. Cucinotta, F. A.; Katz, R.; and Wilson, J. W.: Radial Distribution of Electron Spectra From High-Energy Ions. *Radiat. Environ. Biophys.*, vol. 37, 1998, pp. 259–265.

8. Seltzer, Stephen M.; and Berger, Martin J.: Bremsstrahlung Spectra From Electron Interactions With Screened Atomic Nuclei and Orbital Electrons. *Nucl. Inst. & Meth. Phys. Res.*, vol. B12, 1985, pp. 95–134.

9. Storm, E.; and Israel, H. I.: Photon Cross Sections From 1 keV to 100 MeV for Elements Z = 1 to Z = 100. *Nucl. Data Tables*, vol. 7, 1970, p. 573.

10. Halbleib, J. A., et al.: *ITS Version 3.0: The Integrated TIGER Series of Coupled Electron/Photon Monte Carlo Transport Codes.* SAND91-1634, Radiation Safety Information Computation Center, March 1992.

11. Stassinopoulos, E. G.: The Geostationary Radiation Environment. *J. Spacecraft*, vol. 17, no. 2, 1980, pp. 145–152.
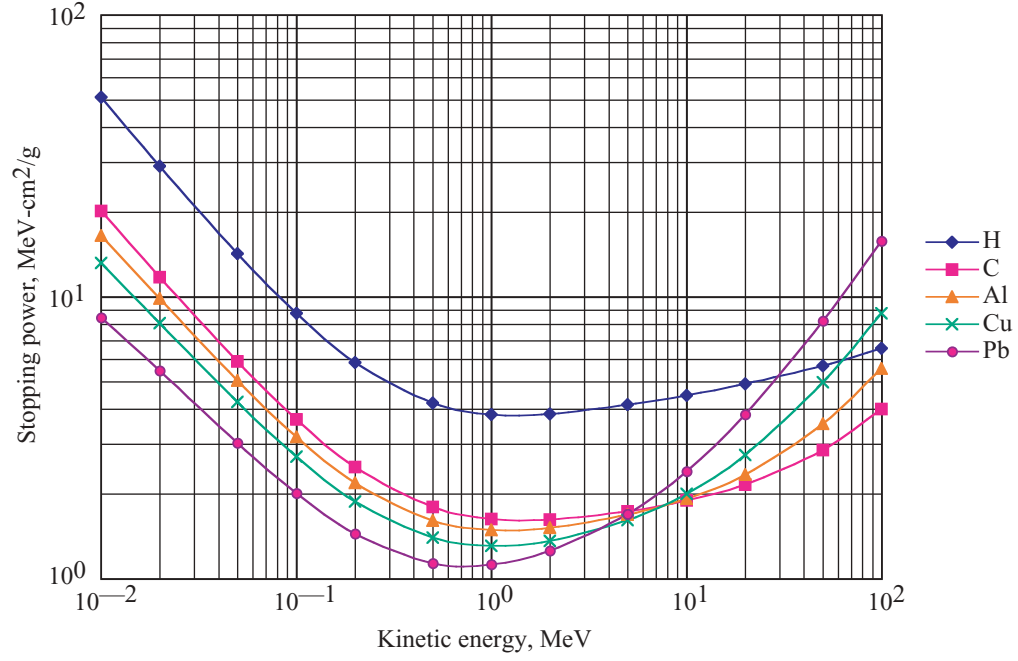
Figure 1. CSDA stopping powers for selected elemental species.
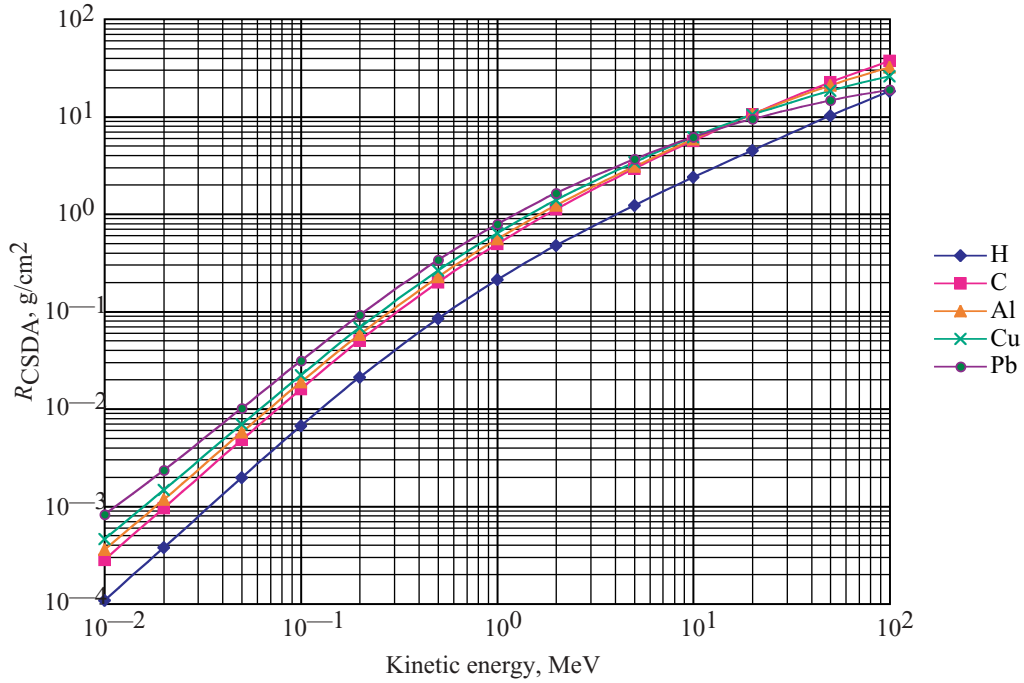
Figure 2. CSDA ranges (R_{CSDA}) for selected elemental species.
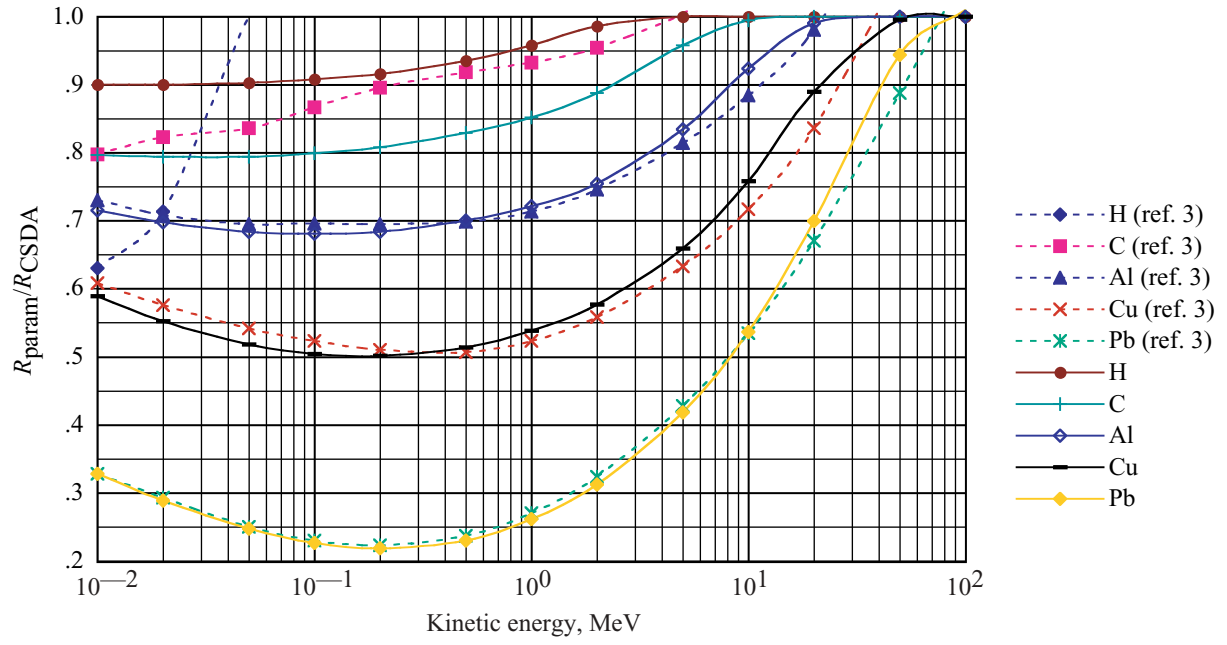
Figure 3. Ratios of parameterized ranges (R_{param}) to CSDA range for selected elemental species. Solid curves are present study curve fittings.

11
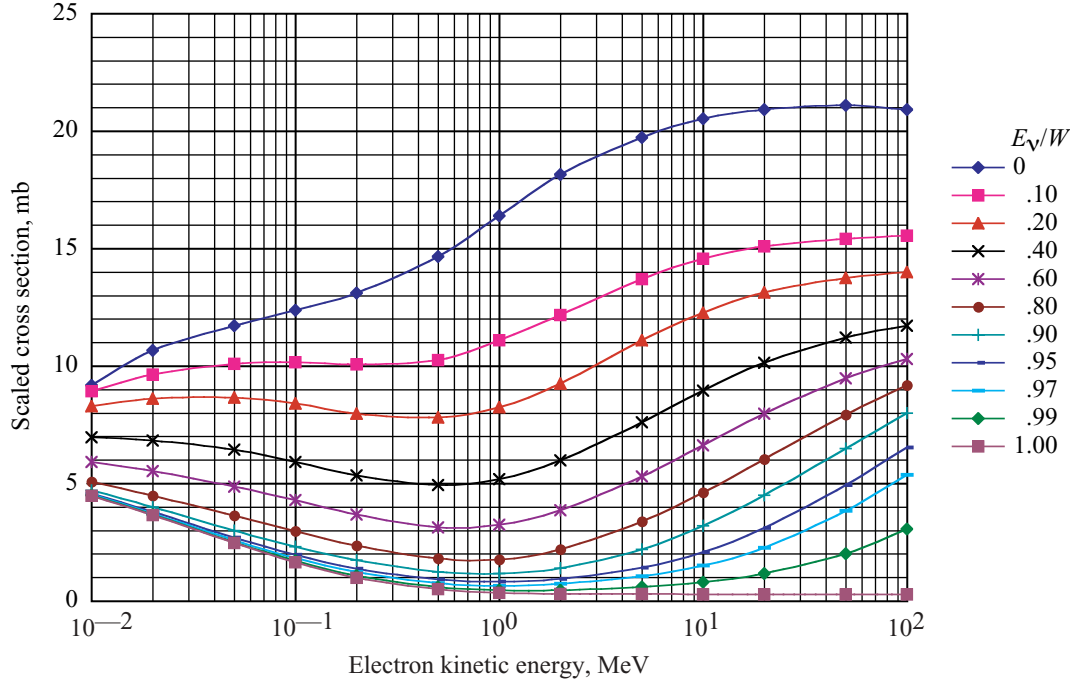
(a) Carbon (Z = 6).
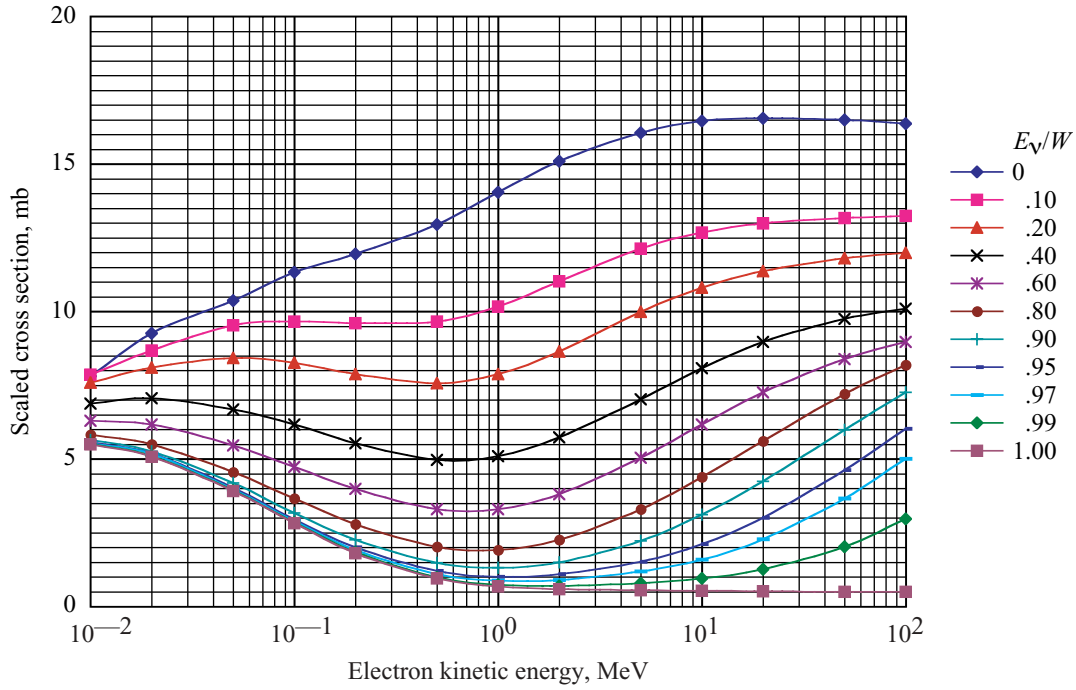
(b) Aluminum (Z = 13).

Figure 4. Scaled photon production differential cross sections versus electron energy for parameter values of energy ratio of emitted photon to incident electron (E_ν/W).
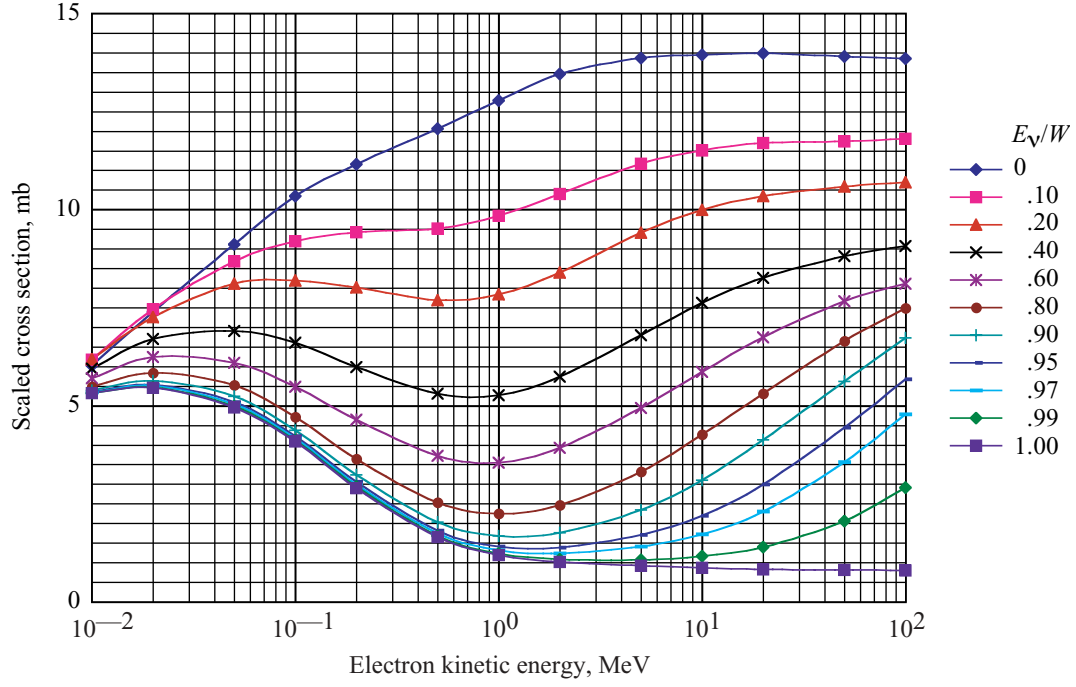
(c) Copper (Z = 29).
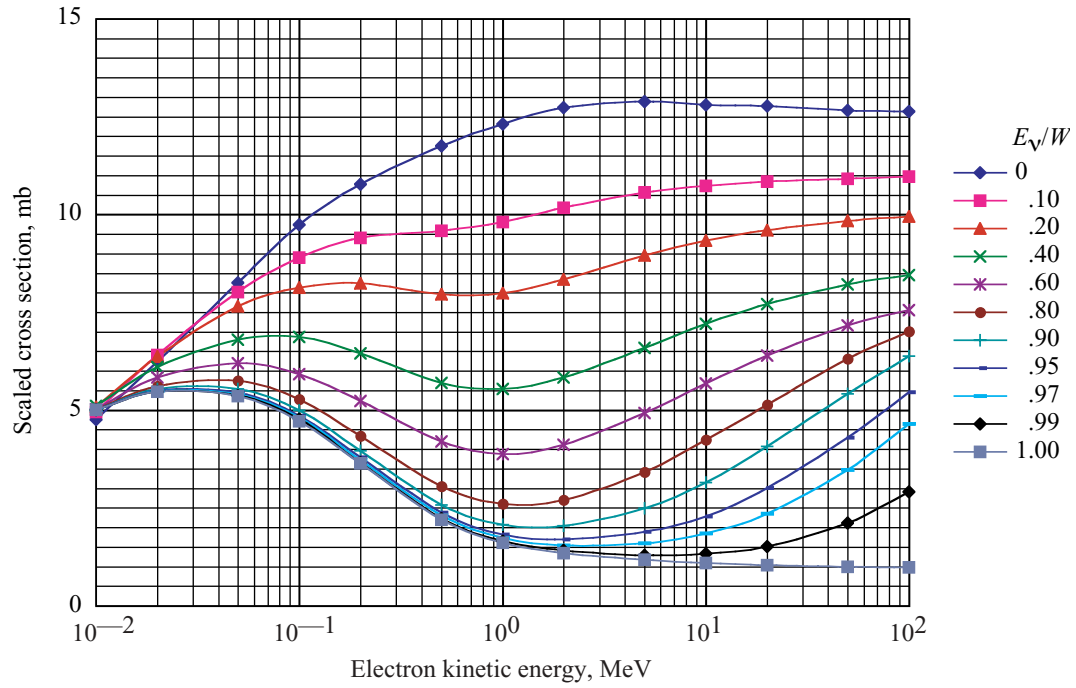
(d) Silver (Z = 47).

Figure 4. Continued.

13
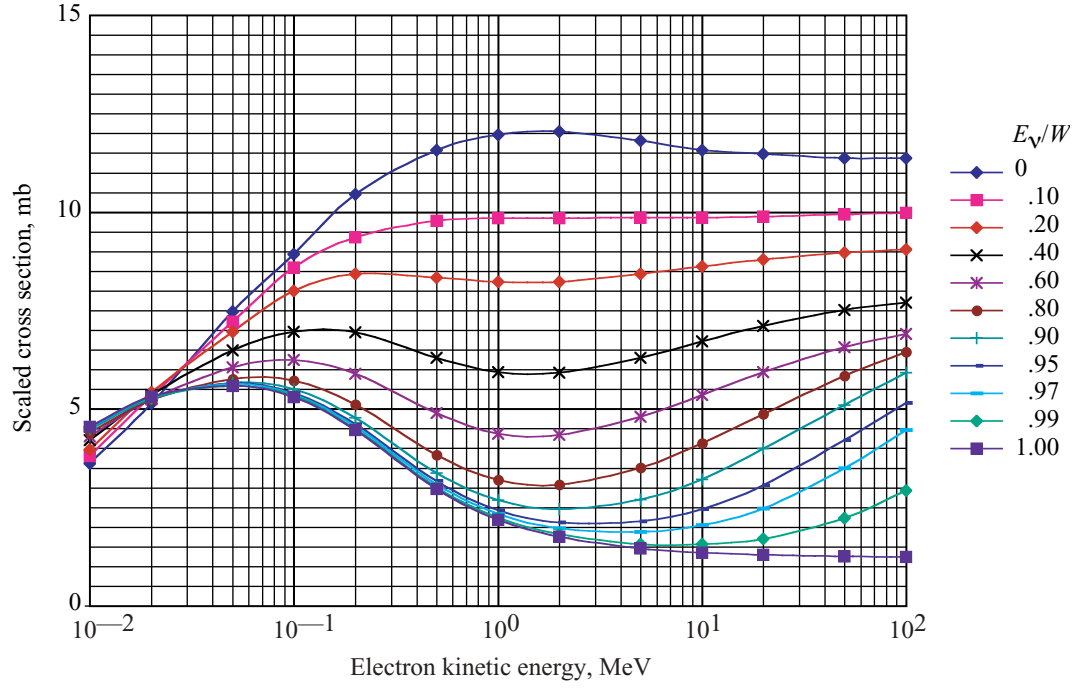
(e) Tungsten (Z = 74).
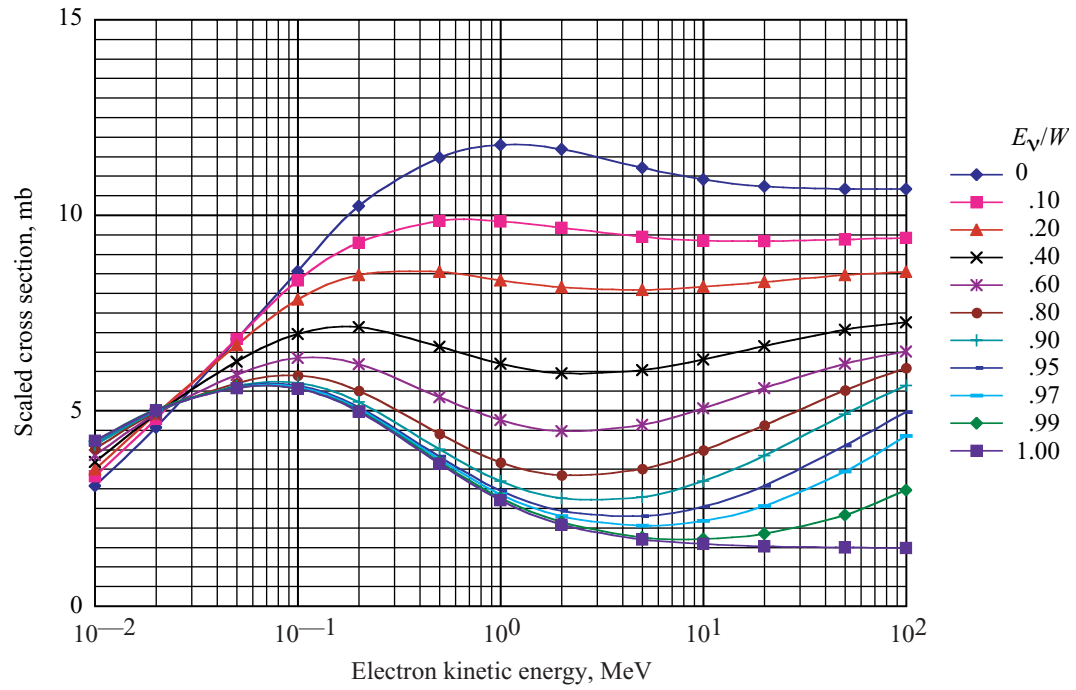
(f) Uranium (Z = 92).

Figure 4. Concluded.

14
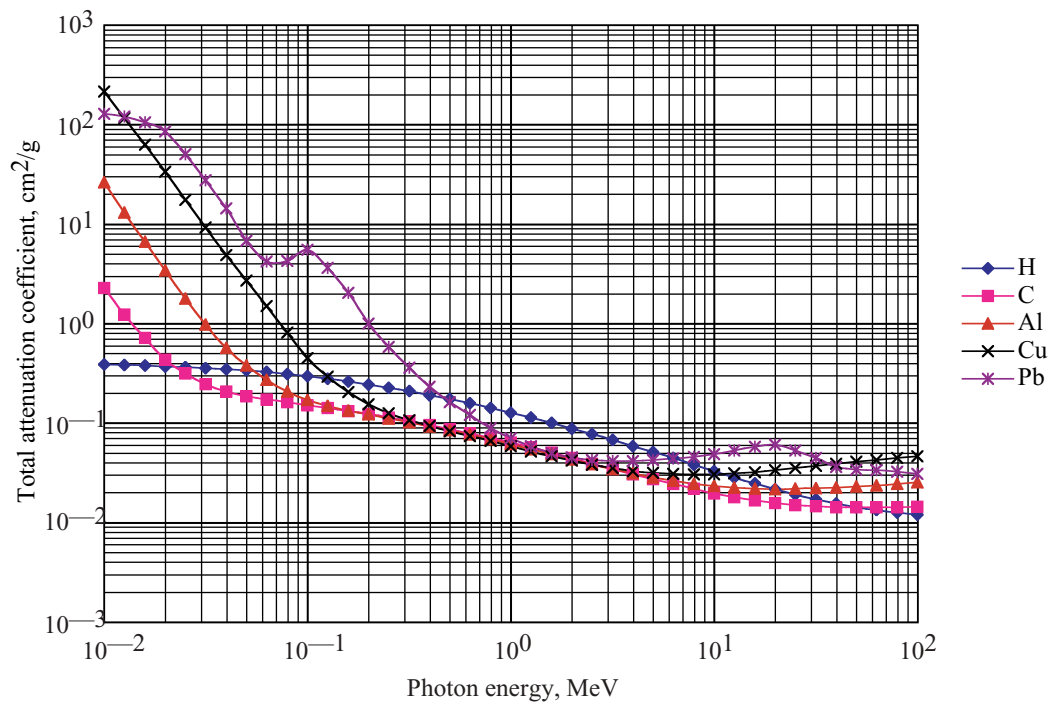
Figure 5. Bremsstrahlung total attenuation coefficient for selected elemental species.
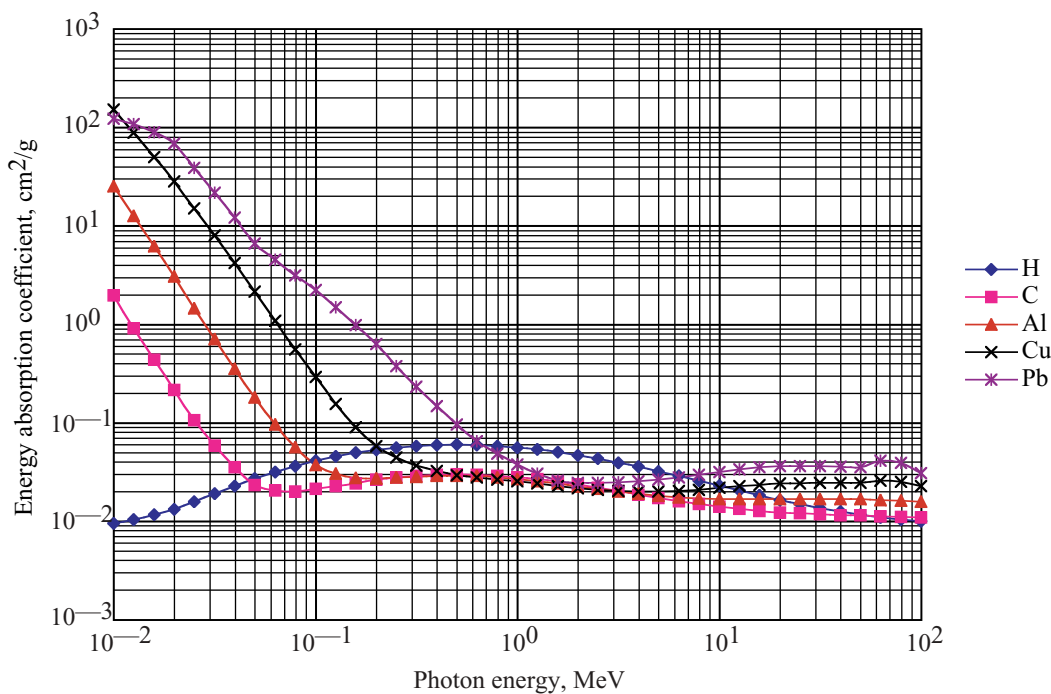
Figure 6. Bremsstrahlung energy absorption coefficient for selected elemental species.
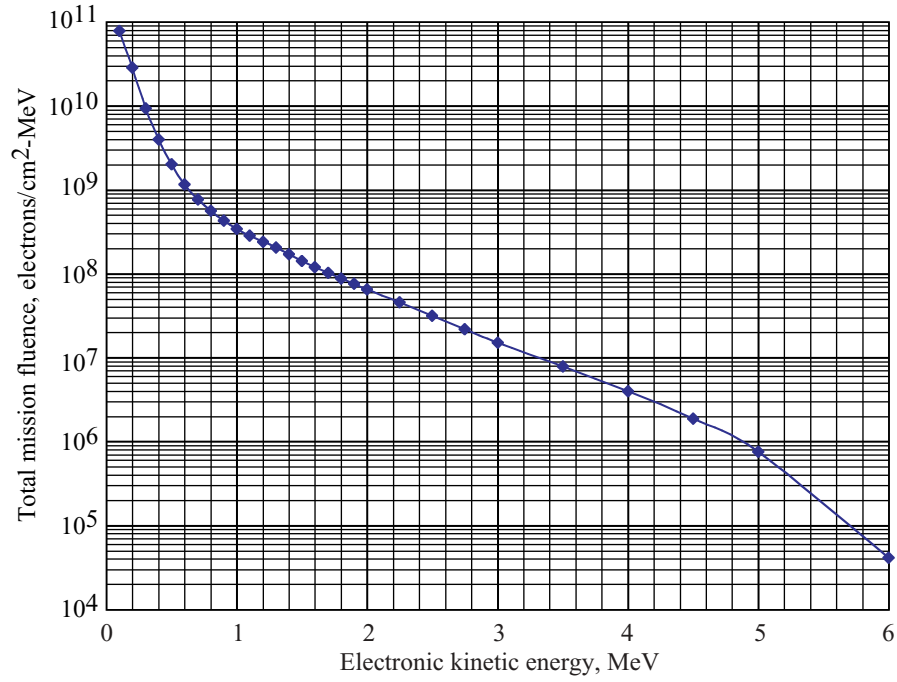
(a) Electron fluence for 10-day mission of STS-63 (394 km at 51.6°).
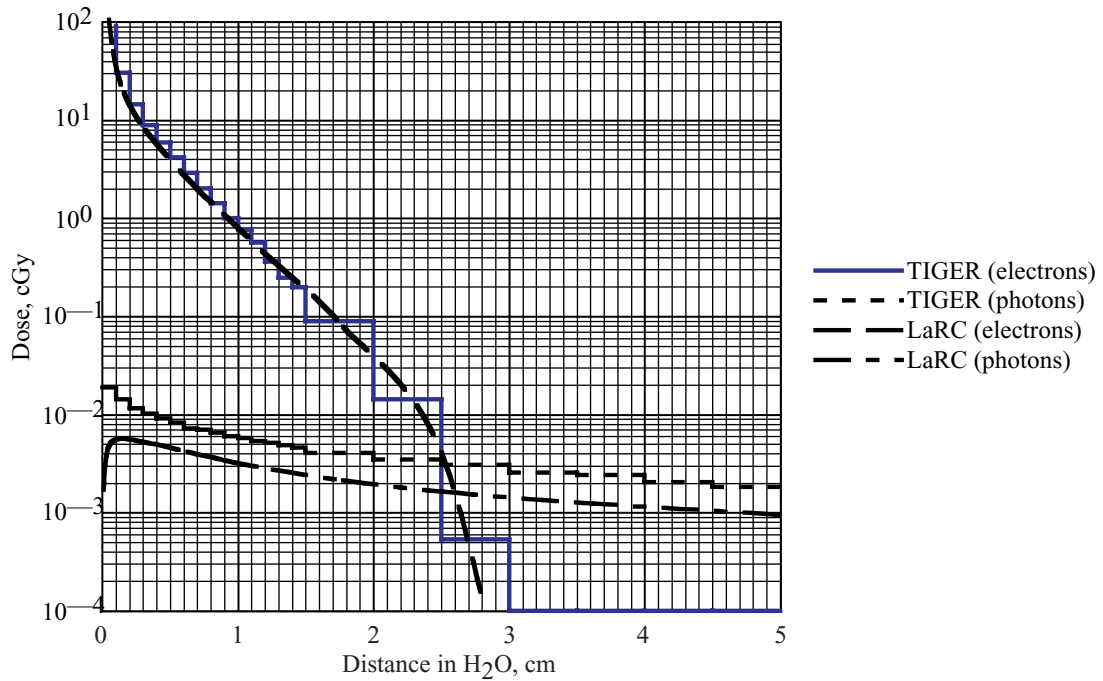
(b) Dose calculation for spectrum in part (a).

Figure 7. Normal incidence propagation results for electrons in H_2O.
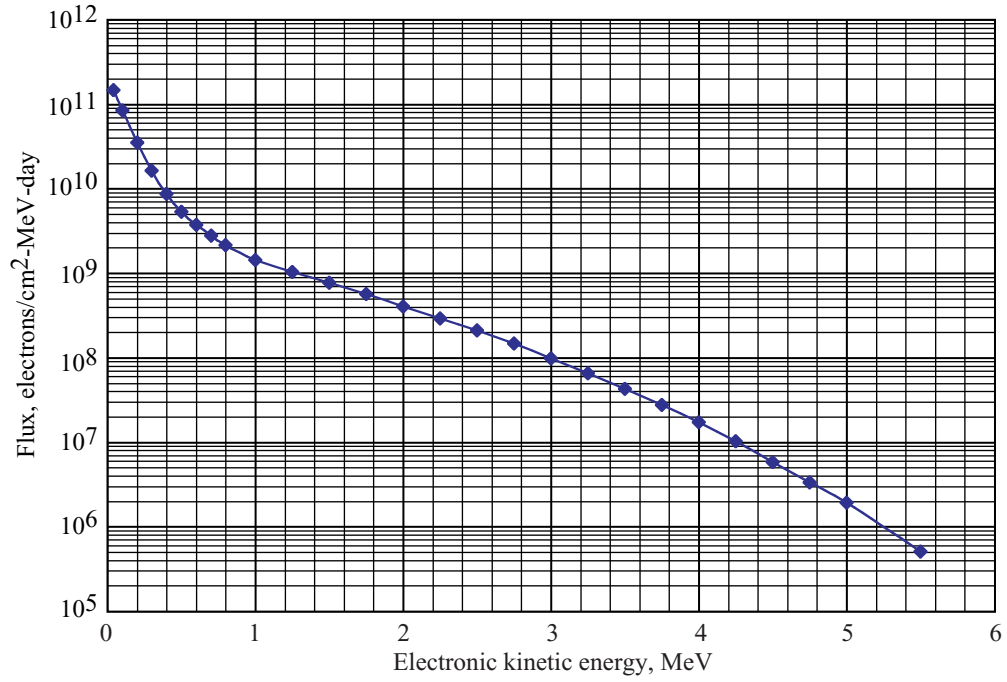
(a) Electron flux spectrum for ISS (400 km at 51.6°) at solar maximum.
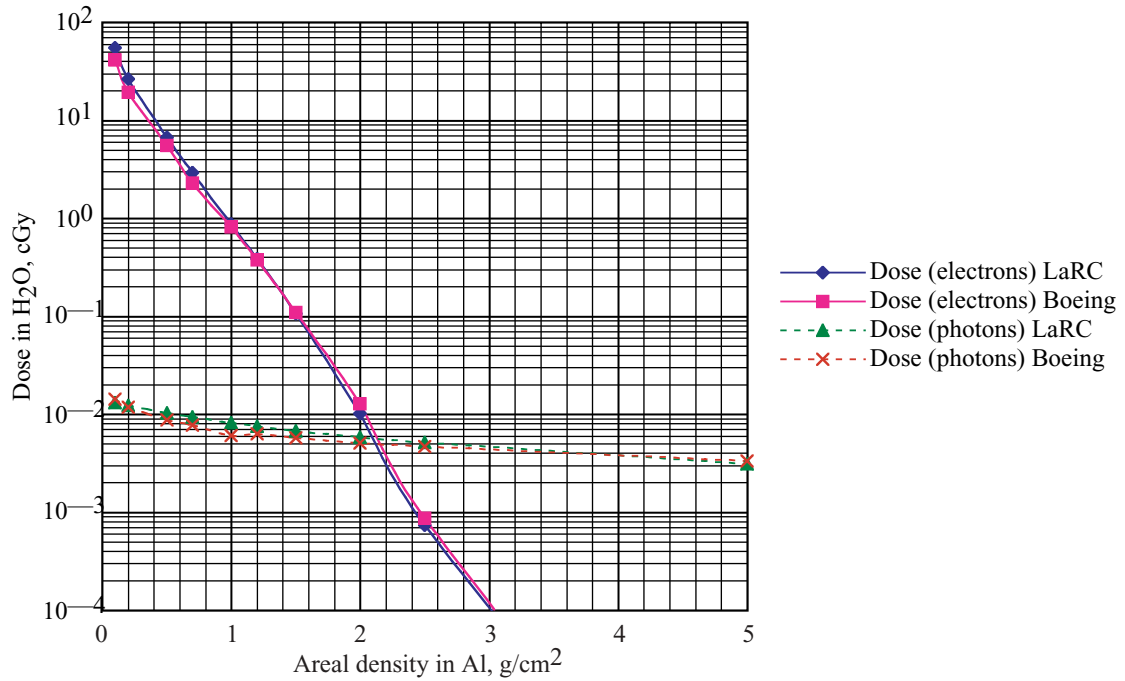
(b) Dose calculation for spectrum in part (a).

Figure 8. Omnidirectional propagation (2π sr) for electrons through Al slab.
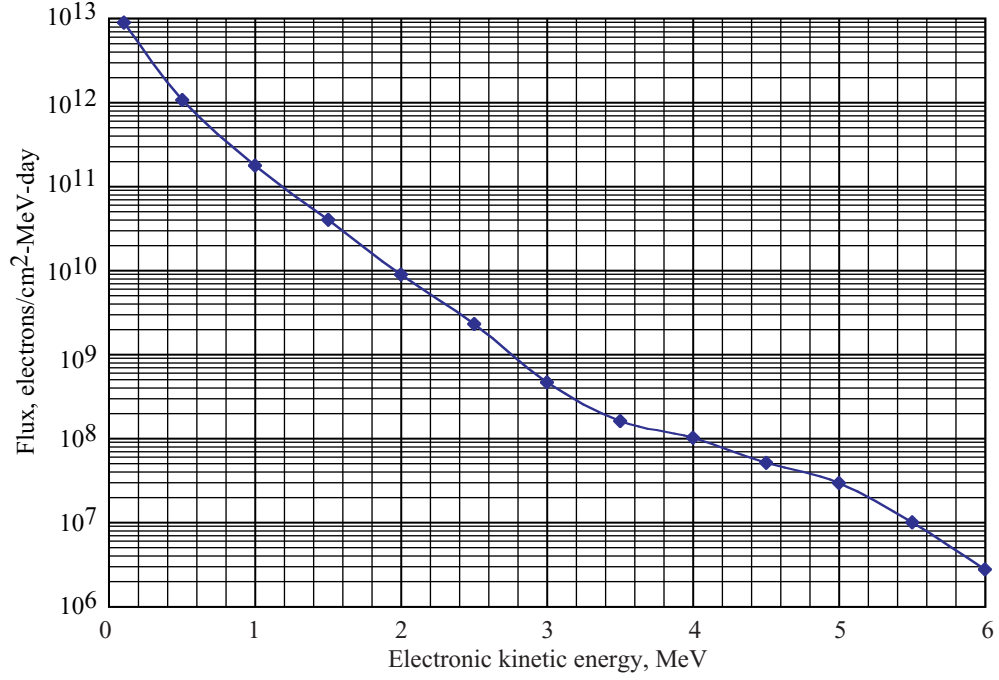
(a) Electron flux spectrum for GEO (35 790 km; 70°W).
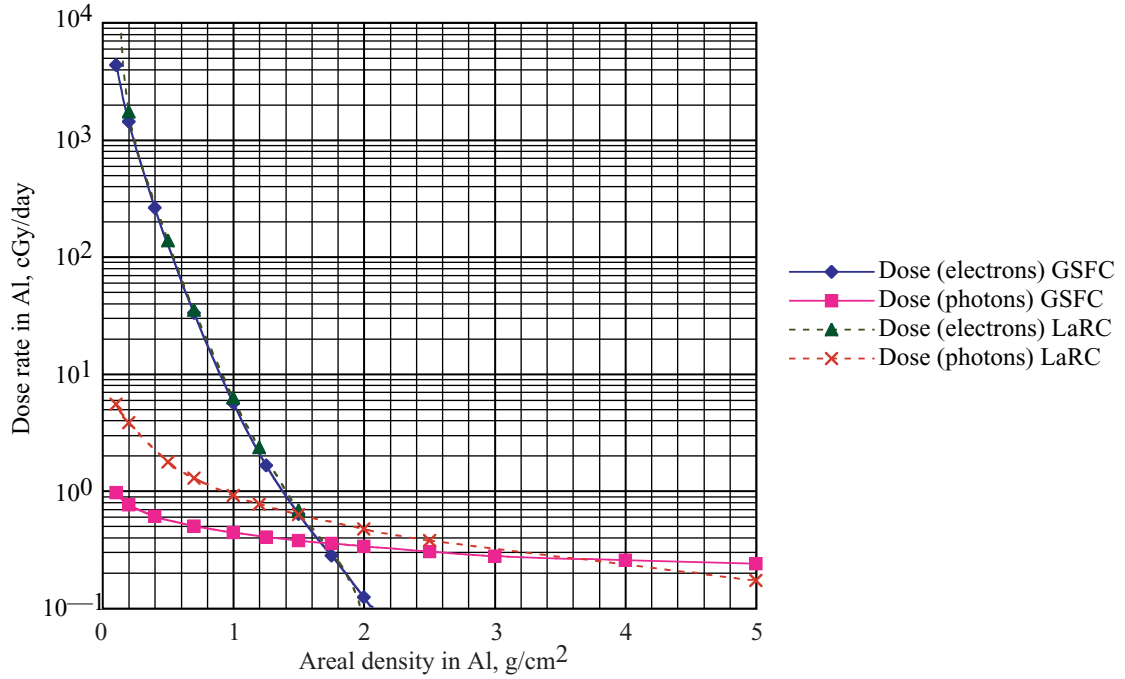
(b) Dose calculation for above spectrum.

Figure 9. Omnidirectional propagation (2π sr) for GEO electrons through Al slab.

18
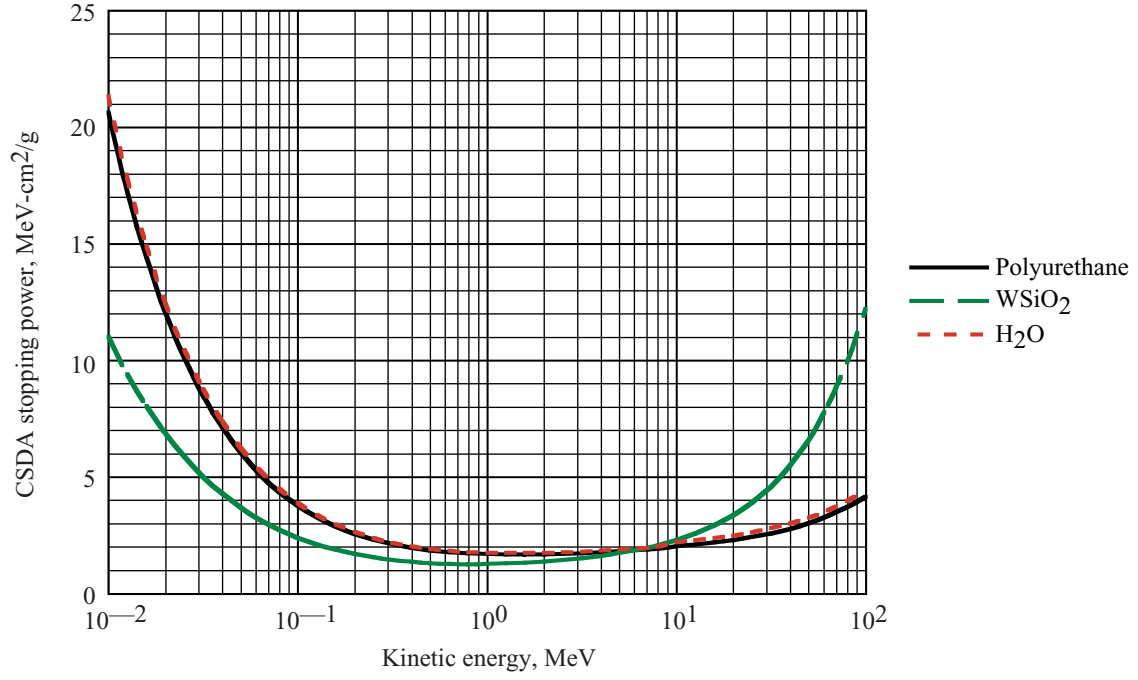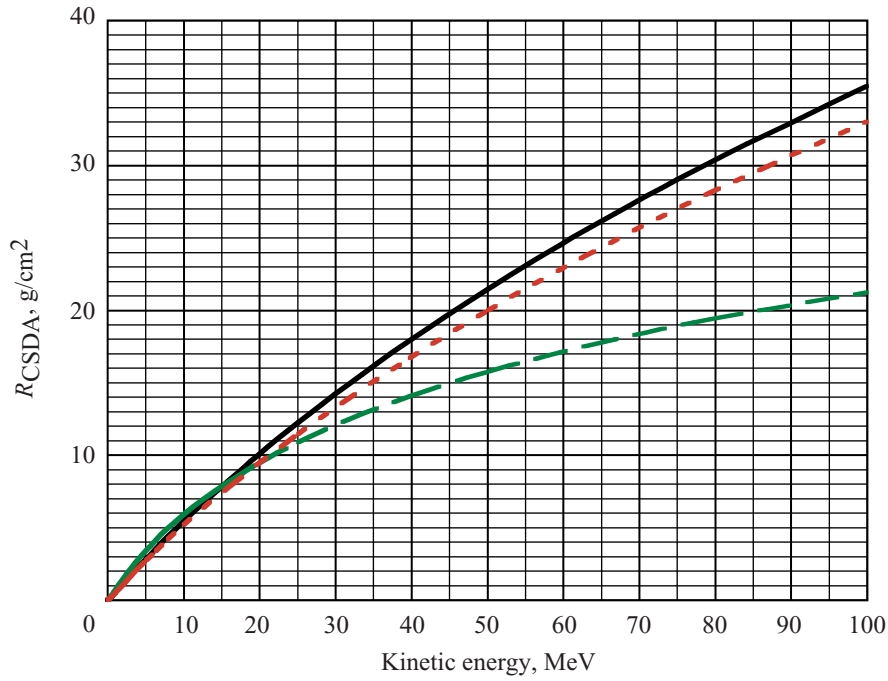
(a) Stopping power.

(b) Range.

Figure 10. Computed stopping powers and ranges for three materials used in sample calculations.
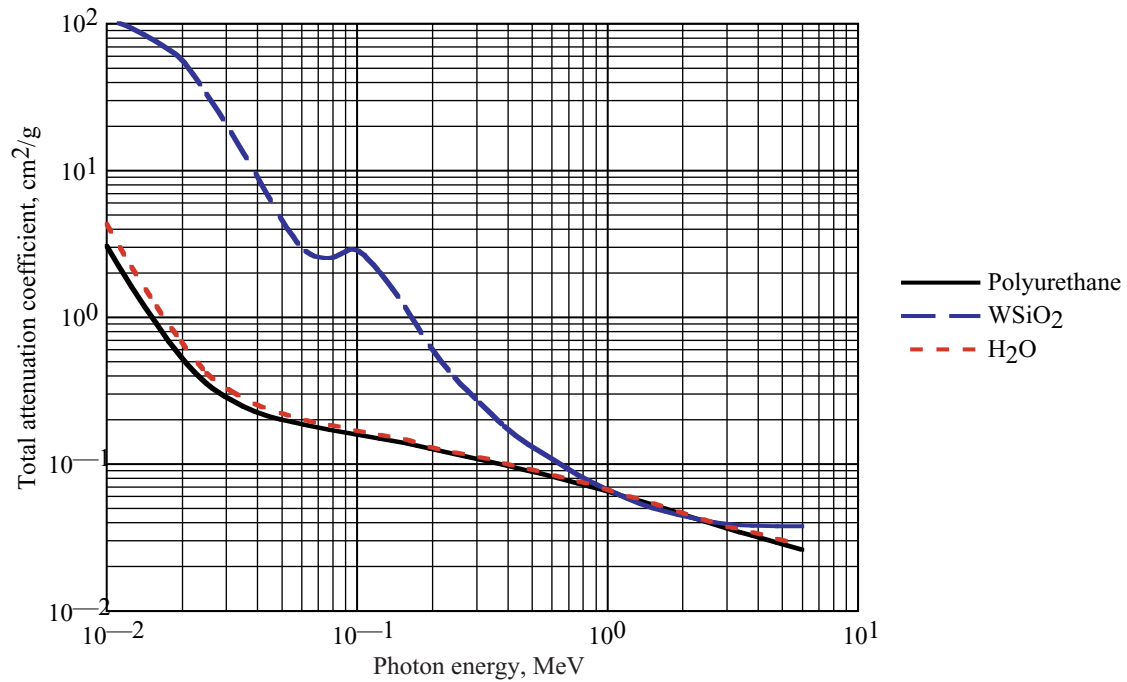
(a) Total attenuation.
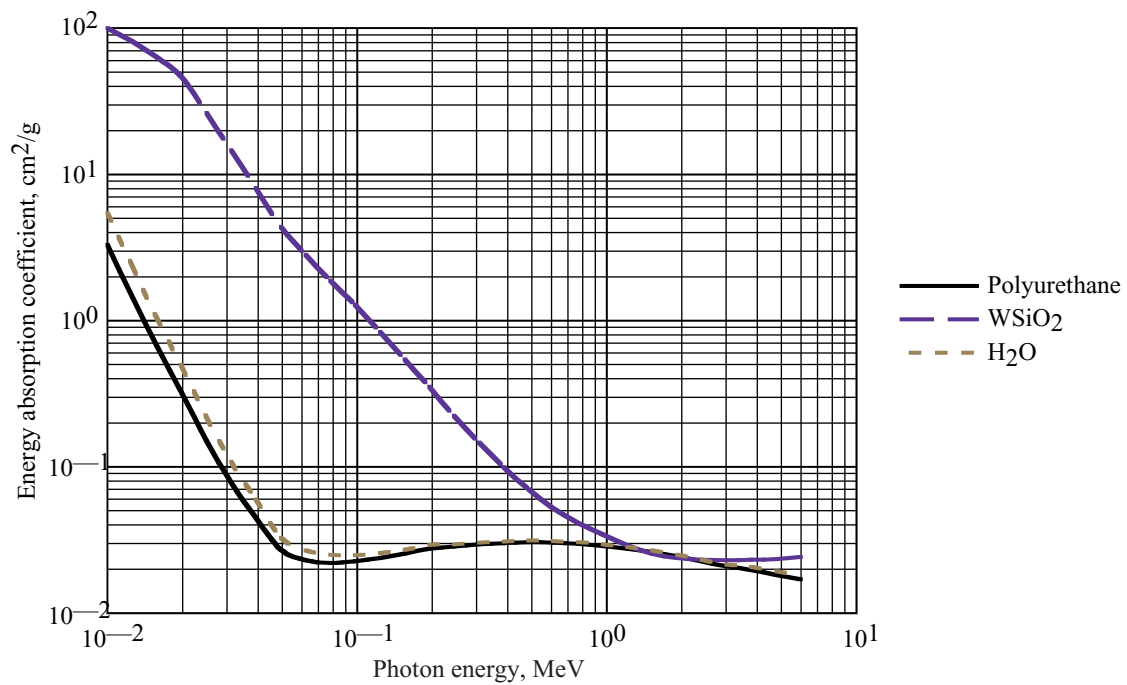
(b) Energy absorption.

Figure 11. Computed photon absorption coefficients for three materials used in sample calculations.
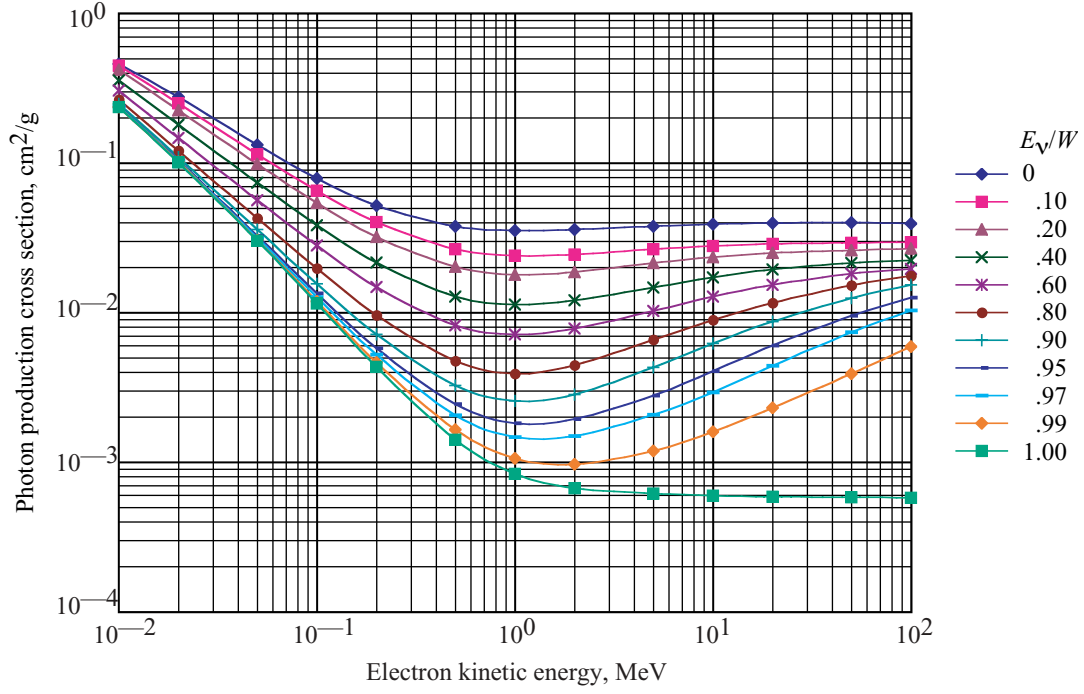
(a) Polyurethane.
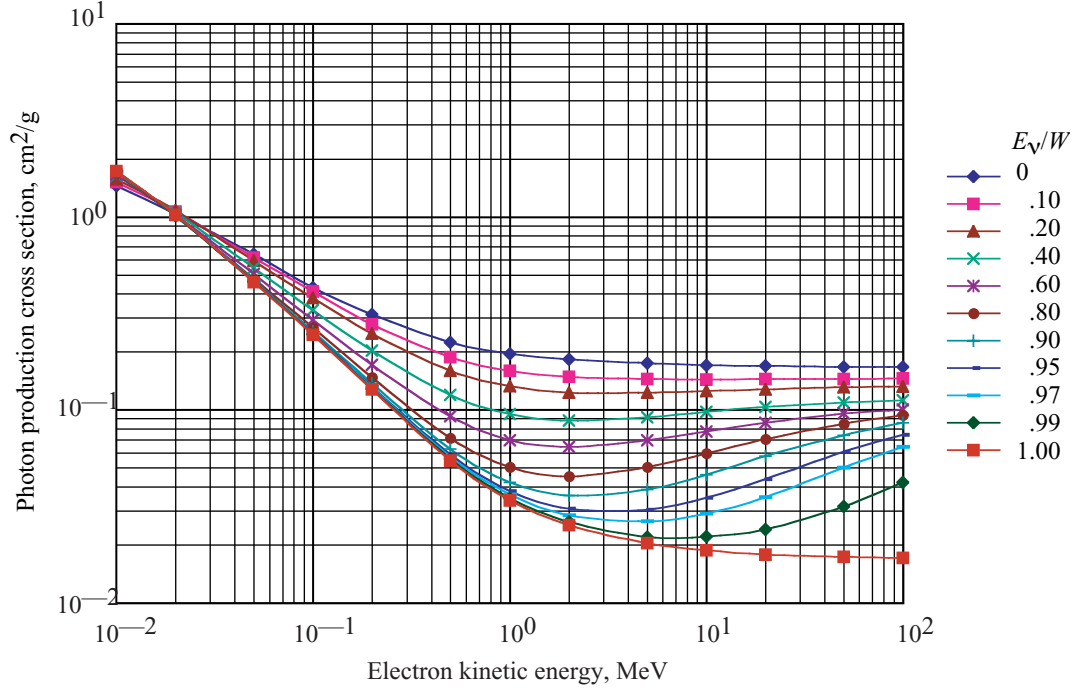
(b) WSiO$_2$ composite.

Figure 12. Computed photon production cross sections for materials used in sample calculations.
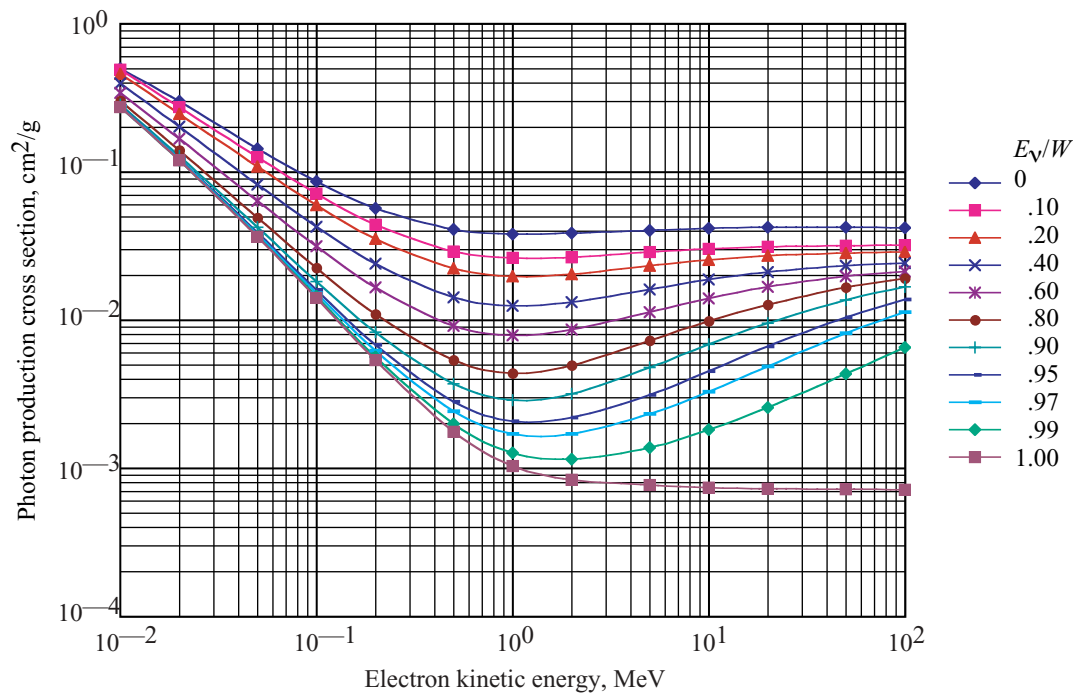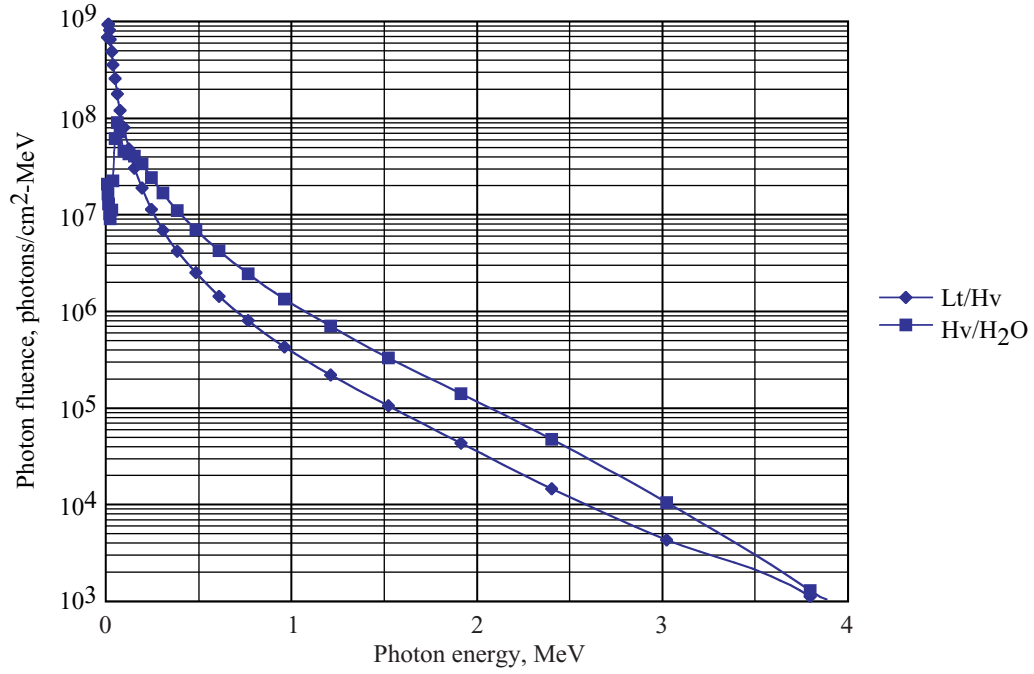
(c) Water.

Figure 12. Concluded.
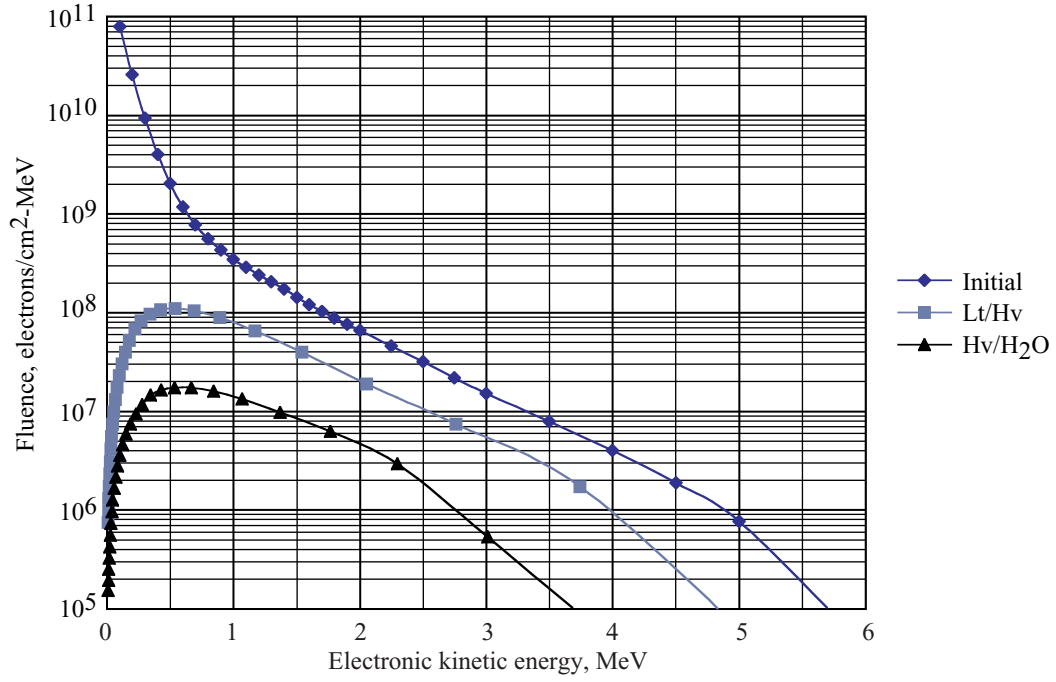
(a) Sequence polyurethane light (Lt)/WSiO$_2$ composite heavy (Hv)/water.
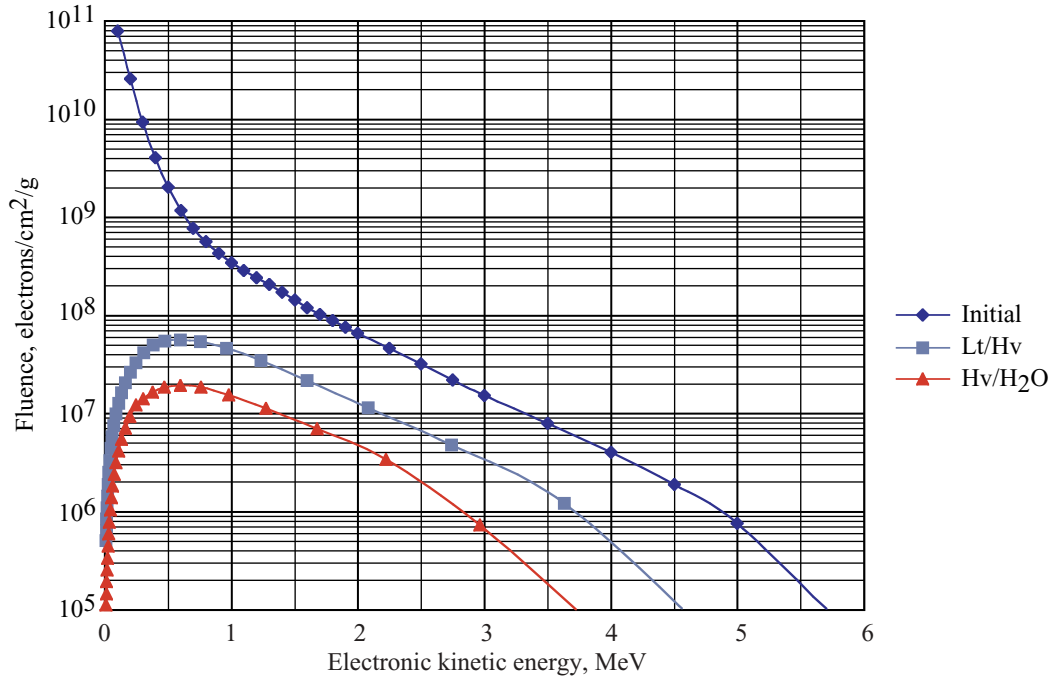
(b) Sequence WSiO$_2$ composite (Hv)/polyurethane (Lt)/water.

Figure 13. Sample calculation of electron fluence spectra for three-layer slab combinations.
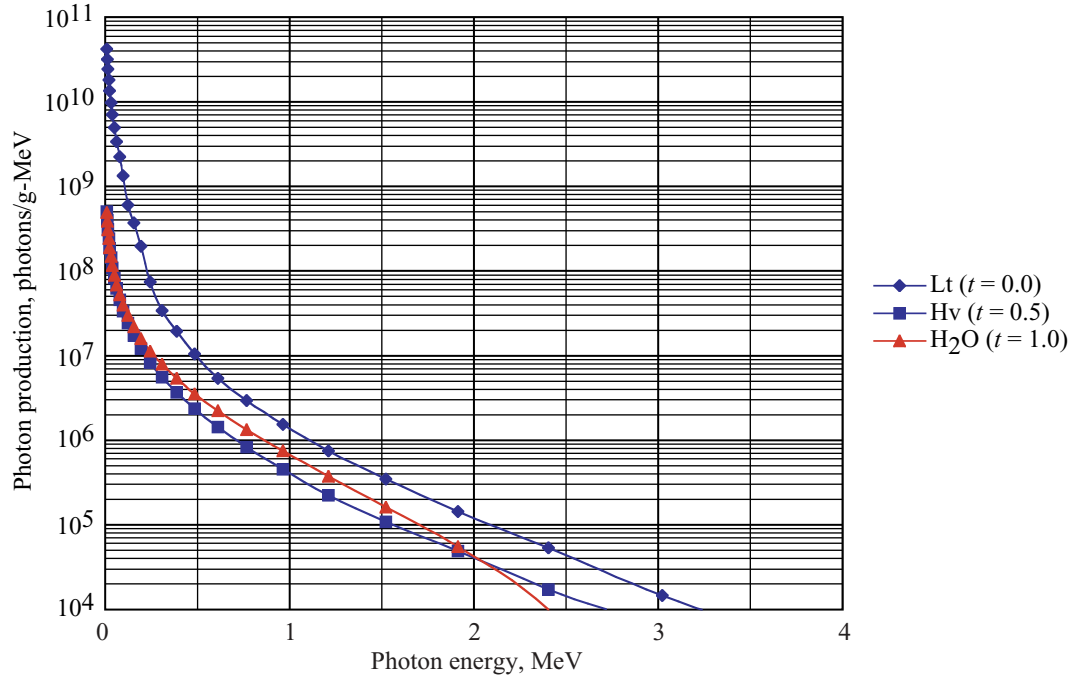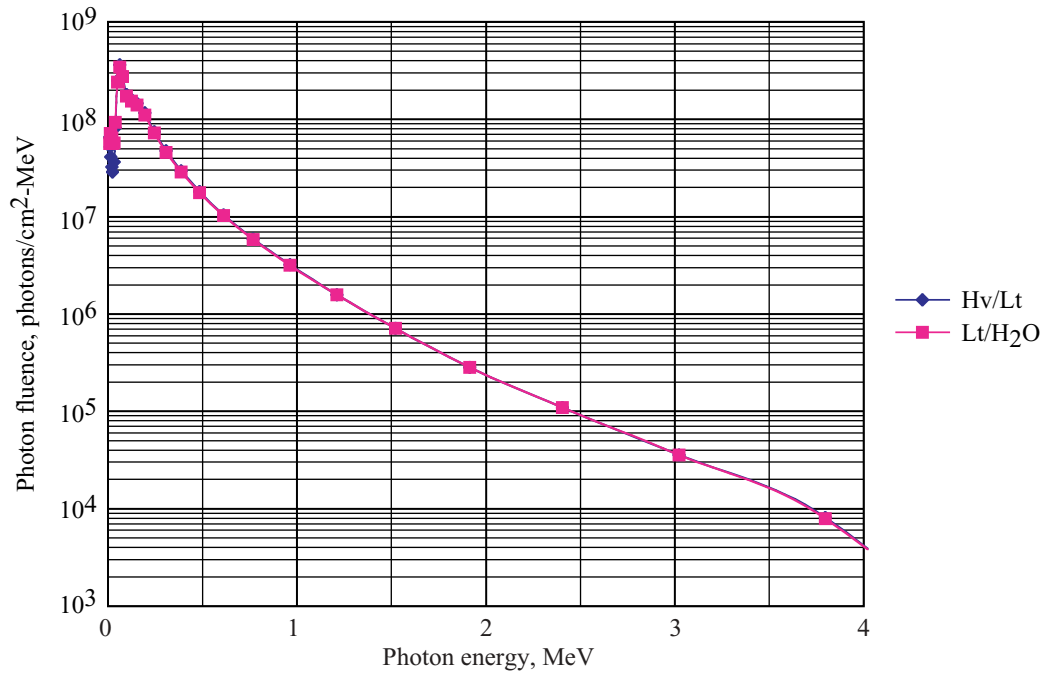
(a) Sequence polyurethane (Lt)/WSiO$_2$ composite (Hv)/water.
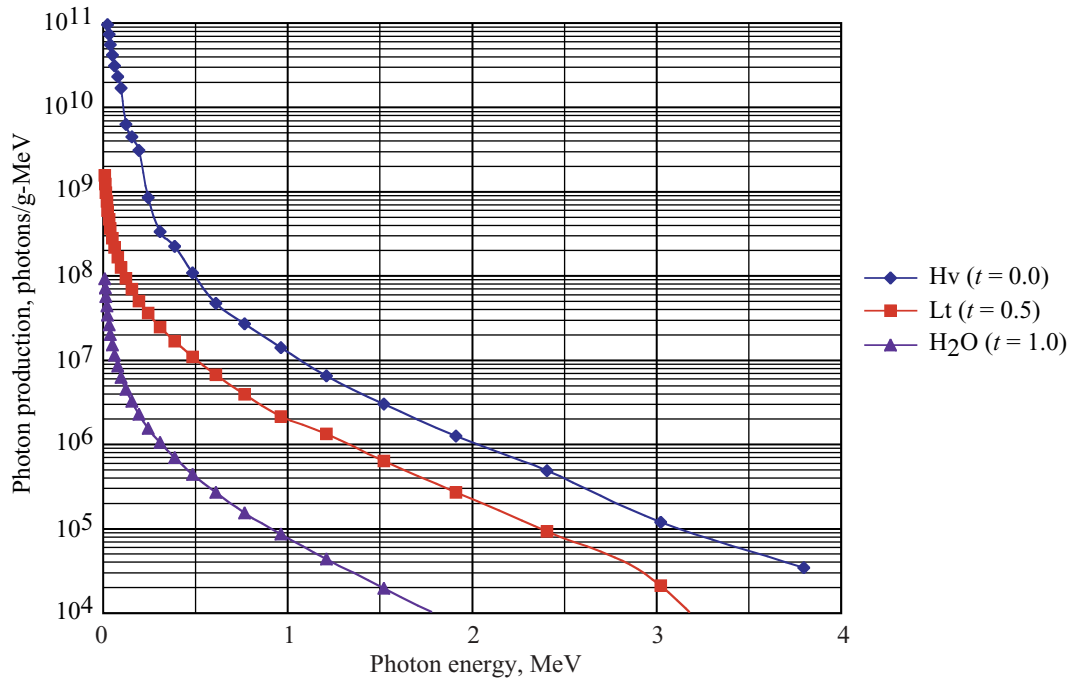
(b) Sequence WSiO$_2$ composite (Hv)/polyurethane (Lt)/water.

Figure 14. Sample calculation of photon source spectra for three-layer slab combinations.
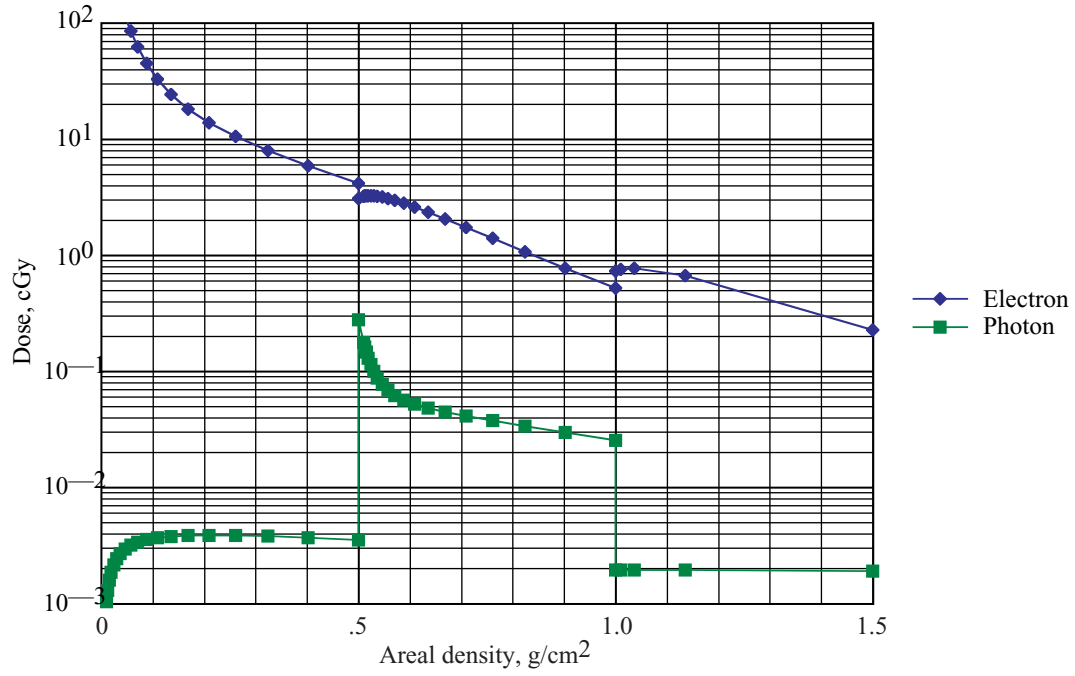
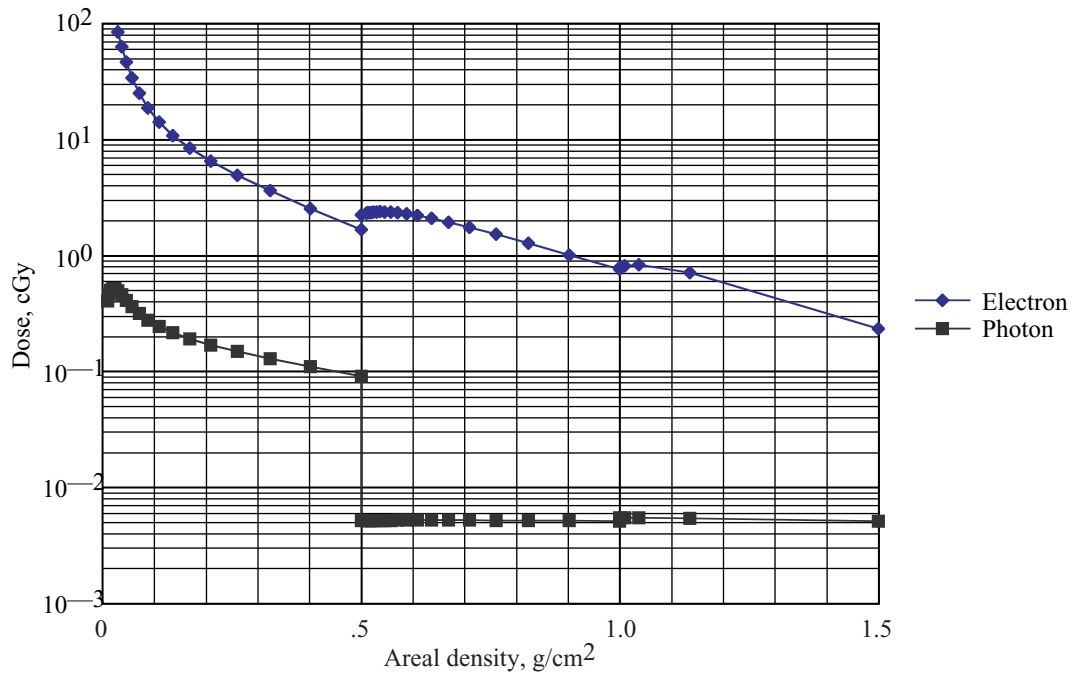(a) Sequence polyurethane (Lt)/WSiO$_2$ composite (Hv)/water.

(b) Sequence WSiO$_2$ composite (Hv)/polyurethane (Lt)/water.

Figure 15. Sample calculation of photon energy spectra for three-layer slab combinations at interior interfaces.

(a) Sequence polyurethane/WSiO$_2$ composite/water.

(b) Sequence WSiO$_2$ composite/polyurethane/water.

Figure 16. Variation of dose (energy deposition) with depth for three-layer slab combinations.

REPORT DOCUMENTATION PAGE

Form Approved
OMB No. 0704-0188

1. AGENCY USE ONLY *(Leave blank)*	2. REPORT DATE	3. REPORT TYPE AND DATES COVERED
	March 2002	Technical Publication

4. TITLE AND SUBTITLE
Transport of Space Environment Electrons: A Simplified Rapid-Analysis Computational Procedure

5. FUNDING NUMBERS
WU 732-50-00-01

6. AUTHOR(S)
John E. Nealy, Brooke M. Anderson, Francis A. Cucinotta, John W. Wilson, Robert Katz, and C. K. Chang

7. PERFORMING ORGANIZATION NAME(S) AND ADDRESS(ES)

NASA Langley Research Center
Hampton, VA 23681-2199

8. PERFORMING ORGANIZATION REPORT NUMBER

L-18155

9. SPONSORING/MONITORING AGENCY NAME(S) AND ADDRESS(ES)

National Aeronautics and Space Administration
Washington, DC 20546-0001

10. SPONSORING/MONITORING AGENCY REPORT NUMBER

NASA/TP-2002-211448

11. SUPPLEMENTARY NOTES
Nealy: Old Dominion University, Norfolk, VA; Anderson: Swales Aerospace Corporation, Hampton, VA; Cucinotta: Lyndon B. Johnson Space Center, Houston, TX; Wilson: Langley Research Center, Hampton, VA; Katz: University of Nebraska, Lincoln, NE; Chang: Christopher Newport University, Newport News, VA.

12a. DISTRIBUTION/AVAILABILITY STATEMENT

Unclassified–Unlimited
Subject Category 93   Distribution: Standard
Availability: NASA CASI (301) 621-0390

12b. DISTRIBUTION CODE

13. ABSTRACT *(Maximum 200 words)*
A computational procedure for describing transport of electrons in condensed media has been formulated for application to effects and exposures from spectral distributions typical of electrons trapped in planetary magnetic fields. The procedure is based on earlier parameterizations established from numerous electron beam experiments. New parameterizations have been derived that logically extend the domain of application to low molecular weight (high hydrogen content) materials and higher energies (~50 MeV). The production and transport of high energy photons (bremsstrahlung) generated in the electron transport processes have also been modeled using tabulated values of photon production cross sections. A primary purpose for developing the procedure has been to provide a means for rapidly performing numerous repetitive calculations essential for electron radiation exposure assessments for complex space structures. Several favorable comparisons have been made with previous calculations for typical space environment spectra, which have indicated that accuracy has not been substantially compromised at the expense of computational speed.

14. SUBJECT TERMS
Space radiation; Electrons; Bremmsstrahlung

15. NUMBER OF PAGES
31

16. PRICE CODE

17. SECURITY CLASSIFICATION OF REPORT	18. SECURITY CLASSIFICATION OF THIS PAGE	19. SECURITY CLASSIFICATION OF ABSTRACT	20. LIMITATION OF ABSTRACT
Unclassified	Unclassified	Unclassified	UL